

EXPERIMENTAL EVIDENCE FOR THE FORMATION OF HIGHLY SUPERHYDROGENATED POLYCYCLIC AROMATIC HYDROCARBONS THROUGH H ATOM ADDITION AND THEIR CATALYTIC ROLE IN H₂ FORMATION

J. D. THROWER¹, B. JØRGENSEN¹, E. E. FRIIS¹, S. BAUCHE^{1,3}, V. MENNELLA², A. C. LUNTZ^{1,4},
M. ANDERSEN¹, B. HAMMER¹, AND L. HORNEKÆR¹

¹ Department of Physics and Astronomy and Interdisciplinary Nanoscience Center (iNANO), Aarhus University, 8000 Aarhus C, Denmark; thrower@phys.au.dk

² Istituto Nazionale di Astrofisica, Osservatorio Astronomico di Capodimonte, Via Moiariello 16, 80131 Napoli, Italy

Received 2012 February 1; accepted 2012 April 2; published 2012 May 18

ABSTRACT

Mass spectrometry measurements show the formation of highly superhydrogenated derivatives of the polycyclic aromatic hydrocarbon molecule coronene through H atom addition reactions. The observed product mass distribution provides evidence also for abstraction reactions resulting in H₂ formation, in agreement with recent IR measurements. Complementary density functional theory calculations confirm the stability of the observed superhydrogenated species toward spontaneous H and H₂ loss indicating that abstraction reactions may be the dominant route to H₂ formation involving neutral polycyclic aromatic hydrocarbons (PAHs). The results indicate that highly superhydrogenated PAHs could well be formed and could act as efficient catalysts for H₂ formation in the interstellar medium in low UV flux regions.

Key words: astrochemistry – ISM: clouds – ISM: molecules – methods: laboratory – photon-dominated region (PDR)

Online-only material: color figures

1. INTRODUCTION

Polycyclic aromatic hydrocarbons (PAHs) are expected to carry 5%–10% of the available interstellar carbon (Hudgins & Allamandola 2005; Tielens 2011) and have received considerable attention over the past 25 years as a result of having been proposed as carriers of the diffuse interstellar bands (Leger & D’Hendecourt 1985; Duley 2006) and the unidentified infrared bands (Leger & Puget 1984; Allamandola et al. 1999). Much of this work has focused on the spectroscopy of PAH molecules with the aim of explaining the observed PAH emission (see Tielens 2008, and references therein). In diffuse cloud environments PAHs are thought to exist in the gas phase, while in dense clouds IR absorption features attributable to PAHs have been observed toward protostellar objects indicating the presence of both gas (Bregman & Temi 2001) and condensed (Chiar et al. 2000) phase PAHs. A number of studies have investigated both the spectroscopy (see, e.g., Allamandola et al. 1989; Bernstein et al. 2005, 2007; Bauschlicher et al. 2010; Boersma et al. 2011) and photochemistry (see, e.g., Bernstein et al. 1999, 2002; Elsila et al. 2006; Bouwman et al. 2009, 2010, 2011b, 2011a) of PAHs within icy grain mantles. Such measurements have suggested a potentially rich interstellar chemistry involving PAH molecules. Furthermore, inclusion of PAHs in dense cloud gas phase chemical networks reveals a strong dependence of the abundance of many molecular species on the presence of PAHs (Wakelam & Herbst 2008). In photodissociation regions (PDRs), PAHs are thought to play a key role in the photoelectric heating of gas by absorbing stellar far-ultraviolet (FUV) photons (Bakes & Tielens 1994) and also have a strong influence on the chemistry of these regions (Bakes & Tielens 1998). In many cases there

is, however, a lack of laboratory data to provide additional insight into these chemical processes and their efficiency under different astrophysical conditions.

One of the key interactions that can be considered is that between PAHs and atomic hydrogen. The potential importance of PAHs in hydrogen chemistry has been suggested by observations of the ρ Oph-W PDR which have revealed a correlation between PAH and H₂ emission (Habart et al. 2003). It was proposed that PAHs might be involved in H₂ formation in PDRs through chemisorption of H atoms on PAHs and small grains (Habart et al. 2004). H₂ formation in PDRs remains poorly understood as the grain surface routes involving physisorbed H atoms, shown experimentally to be efficient under low-temperature dense and diffuse cloud conditions (Katz et al. 1999; Manicò et al. 2001; Hornekær et al. 2003), are no longer efficient at the higher temperatures found in PDRs. Previous theoretical studies have indicated that PAH cations might act as catalysts for H₂ formation (Cassam-Chenaï et al. 1994; Bauschlicher 1998; Le Page et al. 2009). However, the charge state of PAHs in PDRs is strongly dependent on the stellar FUV flux and therefore extinction, A_v . At the PDR surface the charge balance is dominated by PAH⁺, with PAH[−] and PAH⁰ becoming more important with increasing A_v (Bakes & Tielens 1998). Hydrogen addition reactions involving PAHs in all of these charge states may lead to H₂ formation within PDRs. We have considered the possibility of the addition of hydrogen atoms to neutral PAH molecules to form superhydrogenated PAH (HPAH) species. The presence of such species is supported by observations which have revealed aliphatic C–H stretch features at 3.4 μ m alongside the 3.3 μ m aromatic C–H (Bernstein et al. 1996; Sloan et al. 1997). This supports the results of models by Le Page et al. (2003) showing that large PAHs can exist with high degrees of superhydrogenation in many environments. Although the aliphatic C–H stretch can also arise as a result of the presence of alkane side chains, experimentally obtained IR emission spectra of neutral PAHs with additional peripheral H atoms are more consistent with observations (Wagner et al. 2000).

³ Current address: LAMAp/LERMA, UMR8112 du CNRS, de l’Observatoire de Paris et de l’Université de Cergy Pontoise, 5 mail Gay-Lussac, 95000 Cergy Pontoise Cedex, France.

⁴ Current address: Almaden Research Center, IBM, 650 Harry Road, San Jose, CA 95120, USA.

There are very few reports of experiments investigating hydrogen addition to neutral PAHs, with most focusing on PAH and fullerene cations (Petrie et al. 1992; Scott et al. 1997; Le Page et al. 1997; Snow et al. 1998). Previous density functional theory (DFT) calculations by Rauls & Hornekær (2008) suggested that despite the addition of the first hydrogen atom having a barrier of 60 meV, subsequent addition reactions have small or vanishing barriers. These calculations also revealed a catalytic cycle of hydrogen addition and abstraction reactions leading to H₂ formation, as confirmed by Rodríguez et al. (2010). Similar results for the case of H addition to pyrene have been obtained through the calculations of Rasmussen et al. (2011). Fu et al. (2012) have shown experimentally that UV photons can promote the ejection of H₂ molecules from hydrogenated PAHs. H₂ formation through abstraction reactions resulting from exposure of PAHs to atomic hydrogen has been demonstrated by recent infrared (IR) spectroscopic measurements by Mennella et al. (2012). These measurements show that the efficiency of PAHs as catalysts for H₂ formation depends on the degree of hydrogenation. While the (IR) measurements provided evidence for the formation of superhydrogenated PAHs through the appearance of the aliphatic C–H stretching mode an absolute determination of the hydrogenation degree was not possible.

In this article, we examine experimentally the addition of hydrogen atoms to the coronene molecule. By using mass spectrometric techniques we demonstrate that hydrogen addition can lead to the formation of highly superhydrogenated PAH species with masses close to the maximum theoretically possible. We also present DFT calculations that provide further insight into the nature of the superhydrogenated species formed. In addition, we show that the product mass distribution obtained is consistent with abstraction reaction pathways to form H₂ (and HD) being active, in agreement with recent studies (Mennella et al. 2012).

2. EXPERIMENTAL AND CALCULATION DETAILS

The thermal desorption measurements were performed under ultrahigh vacuum (UHV) conditions. Coronene (C₂₄H₁₂) films were grown by thermal evaporation of bulk coronene (Aldrich, sublimed, 99%) using a home-built temperature controlled source operated at 453 K. The source was thoroughly degassed prior to the experiments in order to remove any residual contaminants. Films were grown on a highly oriented pyrolytic graphite (HOPG; SPI grade 1) substrate supported by a Ta mount on a water-cooled copper sample holder. This grade of HOPG has an excellent mosaic spread and large grain sizes. The freshly cleaved surface therefore presents limited defects such as step edges and grain boundaries. The HOPG was cleaved prior to mounting and was annealed to 1300 K under UHV to remove any contaminants. The source was carefully aligned to ensure that coronene dosing on the Ta surface was minimized. In all cases, a substrate temperature of 290 ± 1 K was used. For each measurement, a monolayer of coronene was prepared by exposing the HOPG to the coronene source for 60 s, sufficient to produce a film of the order of 2–3 monolayers thick, followed by annealing to 390 K to desorb the multilayers. In this way, it is possible to directly compare the thermal desorption yields from different measurements. Supplementary scanning tunneling microscopy measurements revealed a well-ordered monolayer of coronene molecules on the HOPG surface following this preparation procedure. The coronene films were exposed to D atoms produced using a hot capillary thermal cracker (Tschersich & von Bonin 1998; Tschersich 2000) operated at ca. 2000 K to dissociate D₂ (Air Liquide, N30,

>99.9%). The D atom flux was estimated within a factor of two to be 6×10^{13} atoms cm⁻² s⁻¹ by considering the operational parameters (capillary temperature, feed pressure, distance to target) as discussed by Tschersich & von Bonin (1998) and Tschersich (2000). The thermal desorption was performed by increasing the sample temperature linearly with a rate of 1 K s⁻¹ and desorbing species were detected with a quadrupole mass spectrometer (QMS; Extrel CMS LLC) capable of detecting species with mass-to-charge ratios of up to 500. It was possible to scan the entire mass range of interest ($m/z = 290$ – 360) in ca. 1 s combining good temperature resolution with simultaneous detection of all product species.

The DFT calculations were performed with the real-space projector augmented wave GPAW code (Enkovaara et al. 2010) using the generalized gradient approximation of Perdew et al. (1996) for exchange and correlation. The structures were optimized in a non-periodic cubic cell with vacuum regions of 7.5 Å separating the molecule from the edges of the cell. The grid spacing was 0.18 Å. All calculations were performed spin polarized and vibrational zero-point energies are neglected throughout.

3. RESULTS AND DISCUSSION

In order to compare the evolution of the mass spectral distribution as a function of hydrogen atom fluence, Φ_D , thermal desorption measurements were initially carried out on the as-deposited coronene film, i.e., without subsequent exposure to the D atom beam. The desorption traces for the coronene parent ion ($m/z = 300$) exhibit two peaks at ca. 360 K and ca. 465 K which can be attributed to desorption from multilayers and the coronene monolayer, respectively (Figure 1(a)). Small peaks in other mass channels in the range $m/z = 298$ – 302 could be explained by considering fragmentation (H loss) within the ionization source of the QMS and the natural abundance of ¹³C. Importantly, these desorption features occur at the same temperatures as the parent ion indicating they are associated with the desorption of unreacted coronene molecules. The dotted line in Figure 1(a) indicates the 390 K annealing temperature used to prepare the coronene monolayer prior to D atom exposure.

After exposure to the D atom beam, the subsequent thermal desorption traces showed (1) a reduction in the desorption yield obtained for the parent ion signal at $m/z = 300$ and (2) the appearance of peaks corresponding to other higher mass species. We attribute the higher mass species formed during D atom irradiation of the coronene film to superhydrogenated coronene molecules in a range of hydrogenation states. We note that the desorption yields of the hydrogenated species are not corrected for their QMS detection efficiencies as these are not known for these species. Desorption traces for several masses obtained following exposure to a D atom fluence of 3.29×10^{16} atoms cm⁻², as an example, are shown in Figure 1(b). The $m/z = 300$ peak remains centered at ca. 465 K, as for the unexposed sample, indicating that it arises from unreacted coronene. The higher mass species are observed to shift to lower desorption temperature with increasing Φ_D . This shift likely results from a reduction in binding between the coronene molecule and the HOPG substrate as the size of the π -electron system is reduced through conversion of carbon centers from sp^2 to sp^3 hybridization. Such behavior has been seen previously following hydrogen addition to adsorbed benzene forming more weakly bound cyclohexane (Xi & Bent 1992).

In order to assess the degree of hydrogenation as a function of Φ_D the desorption traces corresponding to each mass in the

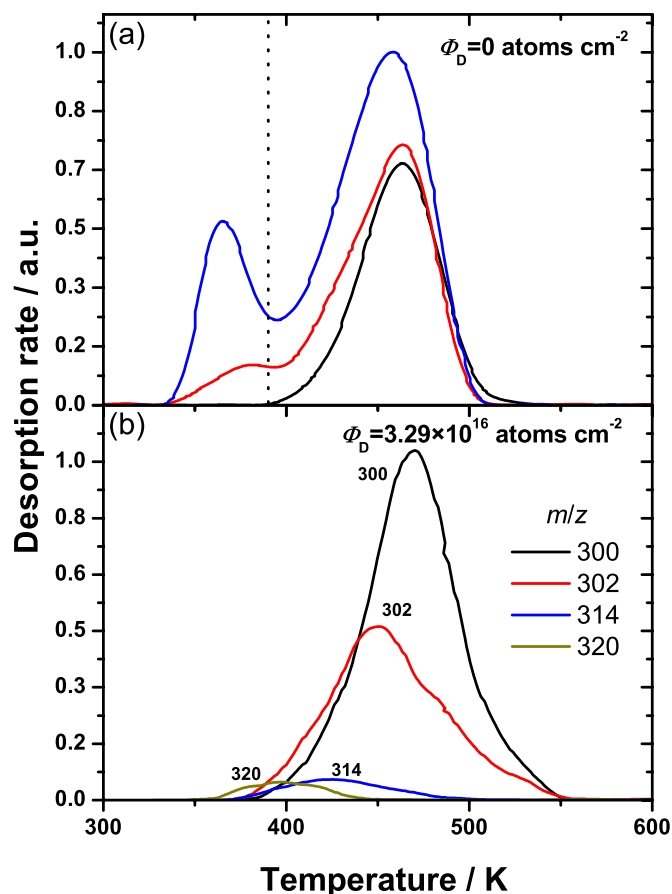


Figure 1. (a) Thermal desorption traces for different exposures of coronene showing the monolayer peak at ca. 465 K and that attributed to multilayers at ca. 360 K. The dotted line indicates the temperature (390 K) to which each film was annealed to prepare a monolayer prior to each D exposure. (b) Desorption traces for several masses obtained following exposure of a monolayer of coronene to a D atom fluence of 3.29×10^{16} atoms cm^{-2} . There is a clear shift to lower desorption temperature for higher masses attributed to superhydrogenated coronene species formed during the D exposure.

(A color version of this figure is available in the online journal.)

range $m/z = 298\text{--}360$ were integrated as a function of time. The resulting product mass distributions were normalized to the total ion signal such that the yields of individual product species are relative to the total desorption yield. The evolution of the product mass distribution with increasing Φ_D is presented in Figure 2 where panel (a) shows the initial mass distribution and panels (b)–(d) show the distribution following increasing exposure to a 2000 K deuterium atom beam for a given D atom fluence. It is clear that hydrogen addition results in a continuous hydrogenation of the coronene molecules, with the mass distribution shifting to higher mass with increasing Φ_D . For the highest fluences the product yield is dominated by species with $m/z > 350$.

The evolution of the mass distribution can be interpreted by considering that the coronene molecule has three possible sites for hydrogen addition (Rauls & Hornekær 2008). The outer edge sites are those to which a hydrogen atom is already attached in the unexposed coronene molecule ($\text{C}_{24}\text{H}_{12}$; 300 amu), inner edge sites are edge sites without a hydrogen atom, and center sites correspond to the carbon atoms in the central ring of the molecule. The calculations performed by Rauls & Hornekær (2008) indicated that addition to center and inner edge sites, as well as outer edge sites, is possible. However, there are no

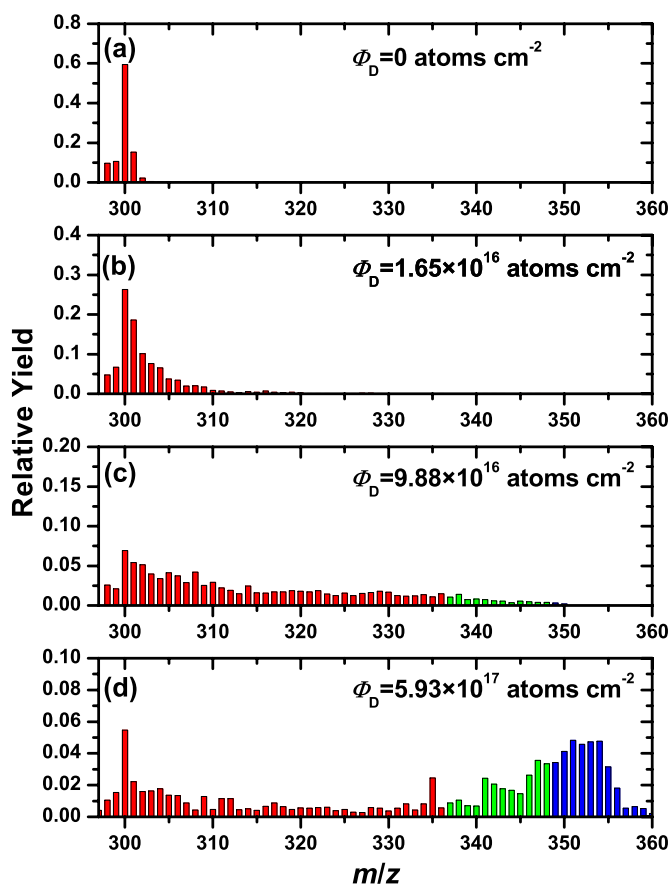


Figure 2. Product mass distributions obtained following exposure of a monolayer of coronene to D atom fluences of (a) 0, (b) 0.165 , (c) 0.988 , and (d) 5.93×10^{17} atoms cm^{-2} . Masses in excess of 336 amu (green (open) and blue (hatched) bars) can only be obtained through addition to center and inner edge sites, i.e., those C atoms in the initial coronene molecule that are not bonded to an H atom. Reactions that replace existing edge site H atoms with D atoms must be in operation to form masses in excess of 348 amu (blue (hatched) bars) providing evidence for abstraction reactions.

(A color version of this figure is available in the online journal.)

reports of experimental evidence for this, and recent IR investigations by Mennella et al. (2012) were not able to distinguish between population of the different sites. Considering the mass distributions in Figure 2 it becomes apparent that outer edge addition alone is insufficient to account for the observed trends as addition of one D atom to each of the 12 outer edge sites would result in a mass of 324 amu. However, exchange reactions in which the initial H atoms on the outer edge sites are replaced with D atoms would result in a mass of 336 amu as indicated by the red (solid) bars in Figure 2. Green (open) bars correspond to masses above 336 amu which are only attainable if D atom addition to center and/or inner edge sites also occurs, i.e., addition to those C atoms in the initial coronene molecule that are not bonded to an H atom. The observation of masses in excess of 348, as shown by the blue (hatched) bars, indicates that all of the processes discussed occur during exposure to the D atom beam. Residual signal for mass 300 at large fluences can be attributed to traces of unreacted coronene desorbing from the Ta sample mount.

Exchange reactions are expected to proceed by first an addition reaction of a D atom to an outer edge site followed by abstraction of the H atom at that site by a second incoming D atom, leading to HD formation (Mennella et al. 2012).

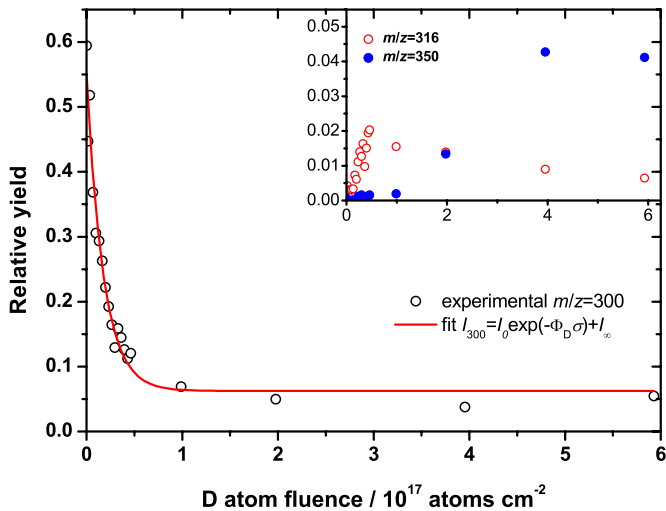


Figure 3. Relative yield of the parent coronene mass 300 signal as a function of D atom fluence representing the conversion of the parent coronene molecule into higher mass species. The decay is well fitted by a single exponential decay function from which a reaction cross-section of $0.7 \pm 0.4 \text{ \AA}^2$ is calculated. The examples in the inset show the more complicated behavior observed for higher mass desorption signals.

(A color version of this figure is available in the online journal.)

Such abstraction reactions resulting from the exposure of carbonaceous materials to atomic hydrogen have been observed previously for graphite (Zecho et al. 2002) and amorphous carbon grain mimics (Mennella 2008). The mass distribution in Figure 2(d) therefore provides clear evidence for both center site hydrogenation and for the catalytic abstraction reactions leading to H_2 (in the present experiment HD or D_2) formation along with a very high degree of superhydrogenation. Reactions between bound D and H have been shown to have barriers in excess of 1 eV (Rauls & Hornekær 2008) and are not expected to occur. The maximum mass observed is close to the theoretical upper limit of one excess D atom per C atom corresponding to 360 amu—the fully deuterated perhydrocoronene molecule (labeled $24\text{H}^{\text{trans}}$ in Figure 4).

From the fluence dependence of the product mass distribution we are able to calculate the cross-section (σ) for the addition of the first deuterium atom, i.e., conversion of mass 300 amu into mass 302 amu. Figure 3 depicts the relative yield of the parent coronene mass 300 signal as a function of D atom fluence. The signal is relative to the total ion count for each fluence and the decay therefore represents the conversion of the parent coronene molecule to higher mass superhydrogenated species. The decay is well fitted by a single exponential decay function of the integrated intensity (I) according to $I = I_0 \exp(-\Phi_D \sigma) + I_\infty$, where the fluence Φ_D is a product of the D atom beam flux (ϕ_D) and exposure time, t . The largest uncertainty is that for the flux (factor of two) resulting in a reaction cross-section of $0.7 \pm 0.4 \text{ \AA}^2$. The examples in the inset show the more complicated behavior observed for higher mass desorption signals. The yields of intermediate-mass fragments go through a maximum as they are formed and then lost through further addition and abstraction reactions. Higher masses show an increasing trend as the system is driven toward the maximum hydrogenation state.

In order to assess the stability of various superhydrogenated coronene molecules, DFT calculations were performed. To mimic coronene adsorbed on a surface with only the top side available for hydrogenation, we attach H atoms only to one side of the molecule. We term these structures NH^{cis} , where

Table 1
Binding Energies per H Atom for Trans- and Cis-hydrogenated Coronene Calculated with Respect to Atomic and Molecular Hydrogen

	$24\text{H}^{\text{trans}}$	24H^{cis}	23H^{cis}	22H^{cis}	21H^{cis}	20H^{cis}	19H^{cis}	18H^{cis}
$E_{b,H}$ (eV/H)	2.62	2.50	2.46	2.52	2.49	2.52	2.48	2.55
E_{b,H_2} (eV/H)	0.35	0.23	0.20	0.25	0.22	0.25	0.21	0.29

N is the number of H atoms attached. We investigated structures with $N = 12$ – 24 , where $N = 24$ corresponds to the fully hydrogenated coronene molecule. For comparison, the perhydrocoronene molecule with 24 H atoms attached to alternating C atoms from both sides (termed $24\text{H}^{\text{trans}}$) was also considered. Selected structures are shown in Figure 4. Binding energies per H atom (shown in Table 1 for selected structures) were calculated with respect to atomic and molecular hydrogen according to the formulae

$$E_{b,H} = (E_{\text{coronene}} + N \cdot E_H - E_{\text{coronene},NH})/N \quad (1)$$

$$E_{b,H_2} = (E_{\text{coronene}} + N/2 \cdot E_{H_2} - E_{\text{coronene},NH})/N, \quad (2)$$

where $E_{\text{coronene},NH}$ and E_{coronene} are the energies of coronene with and without N H atoms attached and E_H and E_{H_2} are the energies of atomic and molecular H. From the binding energies it is immediately seen that the trans-configuration of 24 H atoms is much more stable than the corresponding cis-configuration. The total energy difference equals 24 times the difference in binding energy, which amounts to 2.9 eV. Whereas the trans-configuration remains almost planar except for an alternating up- and down-buckling of the C atoms, the cis-configuration buckles up to form a tubular structure. The buckling in both of these structures results in C–C–H and C–C–C angles close to the ideal tetrahedron value of $109^\circ 5'$, but for H atoms attached to the center sites of the cis-configuration slightly smaller C–C–H angles of around 101° are found. An increased buckling of the molecule would expand these angles, but such buckling is limited by the repulsive interaction of the edge site H atoms on the backside of the molecule, thus explaining the reduced stability compared to the trans-configuration.

In order to obtain the most stable configurations of cis-hydrogenated coronene with $N = 12$ – 23 , up to 12 H atoms were successively removed from the fully hydrogenated structure. We tested a large number of configurations for the remaining H atoms, but not surprisingly the most stable structures with 1–6 H atoms removed were found by removing H atoms from the central carbon ring, where the C–C–H angles are slightly less favorable. The most stable structures with 7–12 H atoms removed were found by subsequently removing H atoms from the inner edge sites. To investigate the stability of the H atoms toward desorption, we plot the energy cost of desorbing an H atom (Figure 5(a)) or an H_2 molecule (Figure 5(b)) from the cis-hydrogenated coronene molecules. Desorbing atomic H is not favorable for any of the structures with energy costs in the range ca. 1–3 eV. The oscillatory behavior in the energies, which is also reflected in the binding energies in Table 1, arises because structures with an even number of H atoms attached are non-magnetic closed-shell systems and more stable than the magnetic open-shell structures with an uneven number of H atoms attached. On the other hand, there are very small costs or even gains associated with the desorption of an H_2 molecule from structures with 24, 23, 20, or 19 attached H atoms. Thus, assuming that the barriers for desorption of H_2 are sufficiently small, these structures will be unstable toward desorption.

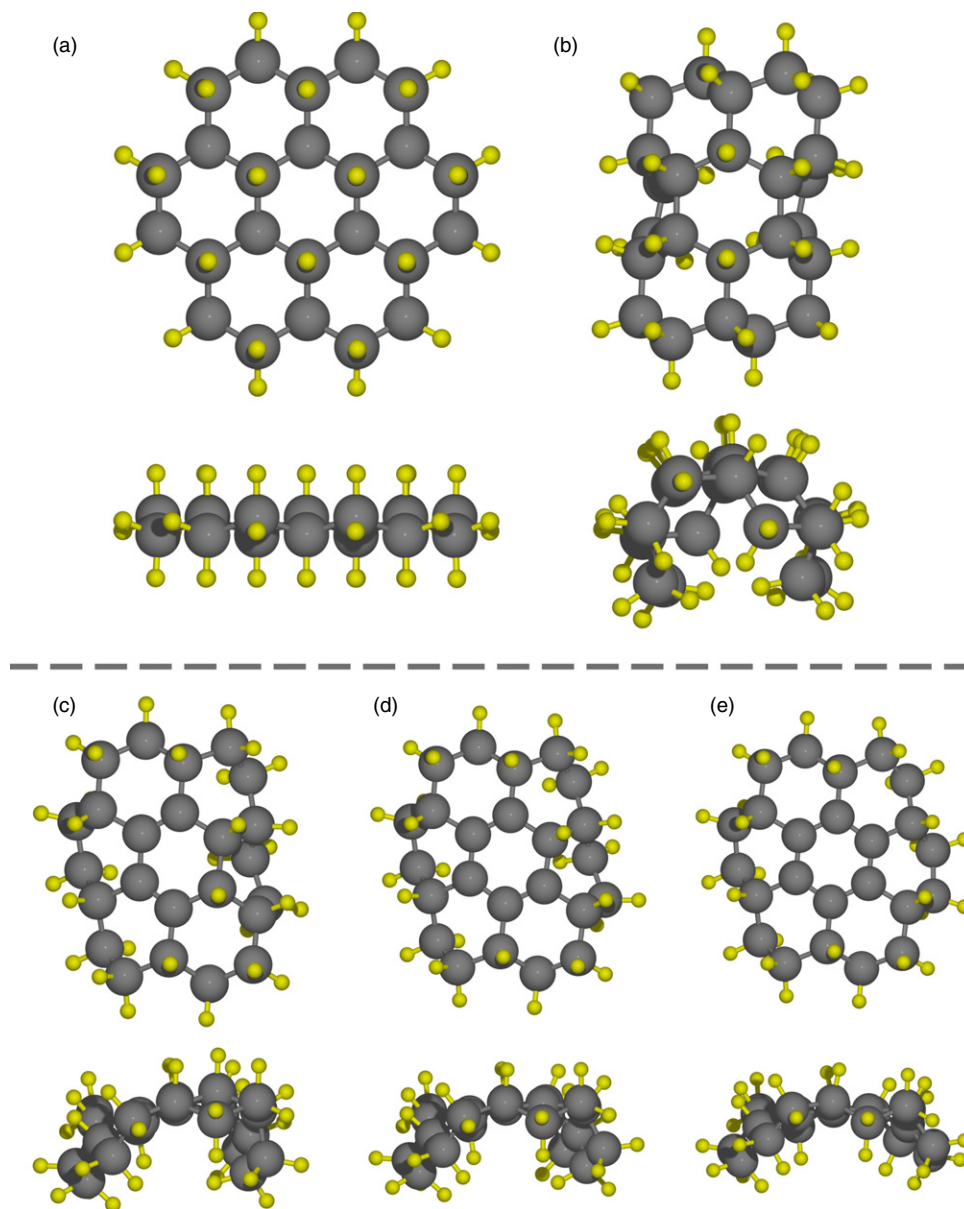


Figure 4. Structures of (a) fully (24H) trans-hydrogenated coronene (perhydrocoronene) and the cis-hydrogenated coronene molecules with (b) 24, (c) 20, (d) 19, and (e) 18 attached H atoms. Both top (upper) and side (lower) views are shown. Carbon atoms are shown in dark gray while hydrogen atoms are yellow (light gray). (A color version of this figure is available in the online journal.)

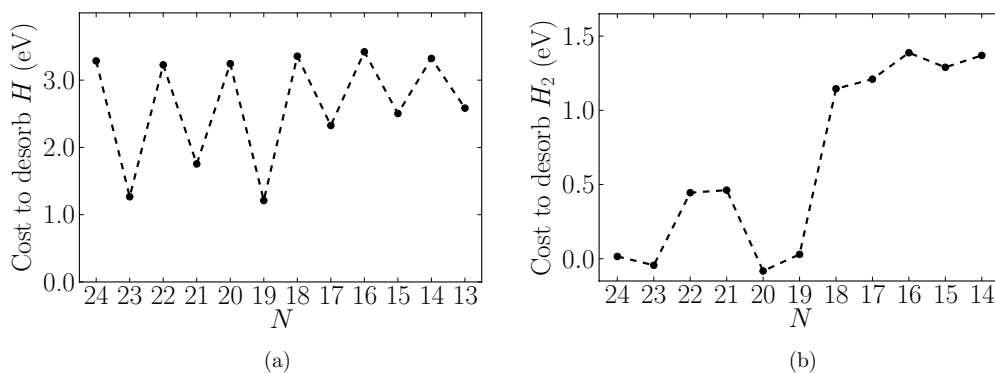


Figure 5. Cost of desorbing an H atom (a) and an H₂ molecule (b) from cis-hydrogenated coronene with N adsorbed H atoms.

The 24H^{cis} and 23H^{cis} structures considered in the calculations correspond to masses of 360 amu and 358 amu in the experiment, assuming complete H/D exchange. The detection

of very few, if any, species with these masses in the experiments reported here may well indicate that these molecules are unstable to D₂ desorption as suggested by the calculations. The

presence of clear signals at 351 and 352 amu may indicate the presence of a barrier to D₂ desorption, possibly related to the larger change in geometry going to structures without center site hydrogenation. The greater stability of the remaining structures with hydrogenated center sites (21H^{cis} and 22H^{cis}) toward H₂ desorption is consistent with the peak in the observed mass distribution at masses corresponding to these structures. It is important to note, however, that the experimentally observed mass distribution is complicated by the presence of abstraction reactions and the possible desorption of higher mass species as a result of reduced adsorption energy. This latter effect manifests itself as a decay in the total ion signal and warrants further investigation. Nevertheless, the results of the calculations support the attribution of the detected higher mass species to superhydrogenated coronene molecules and show that while some extent of double-sided hydrogenation cannot be ruled out in the experiment, single-sided hydrogenation can also lead to the observed mass distributions.

4. CONCLUSIONS

We have investigated the addition of deuterium atoms to the coronene molecule and observed clear evidence for the formation of highly superhydrogenated PAH species. The mass distribution obtained is explained by a combination of addition and abstraction reactions, with the latter acting to form H₂ (here HD and D₂) molecules. These findings support recent infrared measurements that have indicated that neutral PAHs could play an important catalytic role in H₂ formation (Mennella et al. 2012). They also provide the first experimental evidence for the hydrogenation of PAH center sites, as predicted by DFT calculations (Rauls & Hornekær 2008). The experimental observation of product species with such high degrees of superhydrogenation indicates that such species should be formed under interstellar conditions, lending support to observations of IR features previously attributed to superhydrogenated PAHs (Bernstein et al. 1996; Sloan et al. 1997). Given the presence of neutral PAH species within PDRs, the present results may have implications for H₂ formation in such regions. While the results presented here for 2000 K H atoms and in Mennella et al. (2012) for 300 K H atoms demonstrate that PAHs can act as catalysts for H₂ formation over a wide range of H atom temperatures, further investigations are needed to determine the exact dependence of the superhydrogenation level and the cross-sections for molecular hydrogen forming abstraction reactions on the H atom energy. Furthermore, the extent to which interstellar PAHs will become superhydrogenated depends on the rate of UV-induced destruction, which can lead to H atom loss but could also provide a further H₂ formation channel as demonstrated by Fu et al. (2012). A full understanding of the hydrogenation/abstraction process will therefore require measurements of the cross-section for UV-induced desorption.

We acknowledge financial support from the European Research Council under ERC starting grant “HPAH,” No. 208344 and the European Commission’s 7th Framework Programme through the “LASSIE” ITN under Grant Agreement Number 238258.

REFERENCES

- Allamandola, L. J., Hudgins, D. M., & Sandford, S. A. 1999, *ApJ*, 511, L115
 Allamandola, L. J., Tielens, A. G. G. M., & Barker, J. R. 1989, *ApJS*, 71, 733
 Bakes, E. L. O., & Tielens, A. G. G. M. 1994, *ApJ*, 427, 822
 Bakes, E. L. O., & Tielens, A. G. G. M. 1998, *ApJ*, 499, 258
 Bauschlicher, C. W. 1998, *ApJ*, 509, L125
 Bauschlicher, C. W., Jr., Boersma, C., Ricca, A., et al. 2010, *ApJS*, 189, 341
 Bernstein, M. P., Elsila, J. E., Dworkin, J. P., et al. 2002, *ApJ*, 576, 1115
 Bernstein, M. P., Mattioda, A. L., Sandford, S. A., & Hudgins, D. M. 2005, *ApJ*, 626, 909
 Bernstein, M. P., Sandford, S. A., & Allamandola, L. J. 1996, *ApJ*, 472, L127
 Bernstein, M. P., Sandford, S. A., Allamandola, L. J., et al. 1999, *Science*, 283, 1135
 Bernstein, M. P., Sandford, S. A., Mattioda, A. L., & Allamandola, L. J. 2007, *ApJ*, 664, 1264
 Boersma, C., Allamandola, L. J., Bauschlicher, C. W., et al. 2011, in PAHs and the Universe, ed. C. Joblin & A. G. G. M. Tielens (EAS Publications Series, Vol. 46; Les Ulis, France: EDP Sciences), 109
 Bouwman, J., Cuppen, H. M., Bakker, A., Allamandola, L. J., & Linnartz, H. 2010, *A&A*, 511, A33
 Bouwman, J., Cuppen, H. M., Steglich, M., Allamandola, L. J., & Linnartz, H. 2011a, *A&A*, 529, A46
 Bouwman, J., Mattioda, A. L., Linnartz, H., & Allamandola, L. J. 2011b, *A&A*, 525, A93
 Bouwman, J., Paardekooper, D. M., Cuppen, H. M., Linnartz, H., & Allamandola, L. J. 2009, *ApJ*, 700, 56
 Bregman, J. D., & Temi, P. 2001, *ApJ*, 554, 126
 Cassam-Chenaï, P., Pauzat, F., & Ellinger, Y. 1994, in AIP Conf. Proc. 312, Molecules and Grains in Space, ed. I. Nenner (Melville, NY: AIP), 543
 Chiar, J. E., Tielens, A. G. G. M., Whittet, D. C. B., et al. 2000, *ApJ*, 537, 749
 Duley, W. W. 2006, *ApJ*, 639, L59
 Elsila, J. E., Hammond, M. R., Bernstein, M. P., Sandford, S. A., & Zare, R. N. 2006, *Meteor. Planet. Sci.*, 41, 785
 Enkovaara, J., Rostgaard, C., Mortensen, J. J., et al. 2010, *J. Phys.: Cond. Matter*, 22, 253202
 Fu, Y., Szczepanski, J., & Polfer, N. C. 2012, *ApJ*, 744, 61
 Habart, E., Boulanger, F., Verstraete, L., Walmsley, C. M., & des Forêts, G. P. 2004, *A&A*, 414, 531
 Habart, E., Boulanger, F., Verstraete, L., et al. 2003, *A&A*, 397, 623
 Hornekær, L., Baurichter, A., Petrunin, V. V., Field, D., & Luntz, A. C. 2003, *Science*, 302, 1943
 Hudgins, D. M., & Allamandola, L. J. 2005, in IAU Symp. 231, Astrochemistry: Recent Successes and Current Challenges, ed. D. C. Lis, G. A. Blake, & E. Herbst (Cambridge: Cambridge Univ. Press), 443
 Katz, N., Furman, I., Biham, O., Pirronello, V., & Vidali, G. 1999, *ApJ*, 522, 305
 Le Page, V., Keheyian, Y., Bierbaum, V. M., & Snow, T. P. 1997, *J. Am. Chem. Soc.*, 119, 8373
 Le Page, V., Snow, T. P., & Bierbaum, V. M. 2003, *ApJ*, 584, 316
 Le Page, V., Snow, T. P., & Bierbaum, V. M. 2009, *ApJ*, 704, 274
 Leger, A., & D’Hendecourt, L. 1985, *A&A*, 146, 81
 Leger, A., & Puget, J. L. 1984, *A&A*, 137, L5
 Manicò, G., Raguni, G., Pirronello, V., Roser, J. E., & Vidali, G. 2001, *ApJ*, 548, L253
 Mennella, V. 2008, *ApJ*, 684, L25
 Mennella, V., Hornekær, L., Thrower, J., & Accolla, M. 2012, *ApJ*, 745, L2
 Perdew, J. P., Burke, K., & Ernzerhof, M. 1996, *Phys. Rev. Lett.*, 77, 3865
 Petrie, S., Javahery, G., Wang, J. R., & Bohme, D. K. 1992, *J. Am. Chem. Soc.*, 114, 6268
 Rasmussen, J. A., Henkelman, G., & Hammer, B. 2011, *J. Chem. Phys.*, 134, 164703
 Rauls, E., & Hornekær, L. 2008, *ApJ*, 679, 531
 Rodríguez, L. S., Ruetter, F., Sanchez, M., & Mendoza, C. 2010, *J. Mol. Cat. A*, 316, 16
 Scott, G. B. I., Fairley, D. A., Freeman, C. G., et al. 1997, *J. Phys. Chem. A*, 101, 4973
 Sloan, G. C., Bregman, J. D., Geballe, T. R., Allamandola, L. J., & Woodward, C. E. 1997, *ApJ*, 474, 735
 Snow, T. P., Le Page, V., Keheyian, Y., & Bierbaum, V. M. 1998, *Nature*, 391, 259
 Tielens, A. G. G. M. 2008, *ARA&A*, 46, 289
 Tielens, A. G. G. M. 2011, in PAHs and the Universe, ed. C. Joblin & A. G. G. M. Tielens (EAS Publications Series, Vol. 46; Les Ulis, France: EDP Sciences), 3
 Tschersich, K. G. 2000, *J. Appl. Phys.*, 87, 2565
 Tschersich, K. G., & von Bonin, V. 1998, *J. Appl. Phys.*, 84, 4065
 Wagner, D. R., Kim, H., & Saykally, R. J. 2000, *ApJ*, 545, 854
 Wakelam, V., & Herbst, E. 2008, *ApJ*, 680, 371
 Xi, M., & Bent, B. E. 1992, *J. Vac. Sci. Technol. B*, 10, 2440
 Zecho, T., Güttler, A., Sha, X., et al. 2002, *Chem. Phys. Lett.*, 366, 188